PCCP

Accepted Manuscript

ROYAL SOCIETY OF CHEMISTRY

www.rsc.org/pccp

Physical Chemistry Chemical Physics
CREATED USING THE RSC LaTeX PCCP ARTICLE TEMPLATE – SEE www.rsc.org/electronicfiles FOR DETAILS
ARTICLE TYPE www. rsc.org/xxxxxx | XXXXXXXX

Chemical ordering in magic-size Ag-Pd nanoparticles

Davide Bochicchio,[a] Riccardo Ferrando,*[b] Rada Novakovic,[c] Emanuele Panizon,[a] and Giulia Rossi[a]

Received Xth XXXXXXXXXX 20XX, Accepted Xth XXXXXXXXX 20XX
First published on the web Xth XXXXXXXXXX 200X
DOI: 10.1039/b000000x

Chemical ordering in magic-size Ag-Pd nanoalloys is studied by means of global optimization searches within an atomistic potential developed on the basis of Density Functional Theory calculations. Ag-rich, intermediate and Pd-rich compositions are considered for fcc truncated octahedral, icosahedral and decahedral geometric structures. Besides a surface enrichment in Ag, we find a significant subsurface enrichment in Pd, that persists to quite high temperatures as verified by Monte Carlo simulations. This subsurface Pd enrichment is stronger in nanoparticles than in bulk systems and is rationalized in terms of the energetics of the inclusion of a single Pd impurity in an Ag host nanoparticle. Our results can be relevant to the understanding of the catalytic activity of Ag-Pd nanoparticles in those reactions in which subsurface sites play a role.

1 Introduction

Alloy nanoparticles[1], commonly known as nanoalloys, are presently a very active research field, with many recent exciting developments in both experiment and modeling. This growing interest stems from a great variety of possible applications, ranging from catalysis to optics and magnetism. Nanoalloys are even better suited for tailored applications than pure elemental nanoparticles, because they can assume different geometric shapes and different chemical ordering patterns. Possible chemical ordering patterns comprise core-shell, multi-shell, randomly intermixed, intermixed with ordered phases, and quasi-Janus configurations[2–9]. The properties of a nanoalloy strongly depend on its chemical ordering pattern. This has been demonstrated for optical, magnetic and catalytic properties in several cases[1].

The silver-palladium system is of great interest for applications in catalysis, for example in hydrogenation reactions with enhanced selectivity[10,11], where the special role of surface and subsurface hydrogen in the Ag-Pd nanoparticles has been demonstrated. In fact, it has been shown that the addition of Ag to the Pd nanoparticles decreases surface hydrogen much more than subsurface hydrogen, indicating a surface enrichment in Ag[10].

Ag and Pd are miscible in the bulk phase for all compositions, without formation of ordered phases[12]. In Ag-Pd nanoparticles there is experimental evidence in favour of some Ag surface segregation. In fact, Ag-Pd nanoparticles grown by vapor deposition onto thin alumina films show intermixed chemical ordering but their surface is enriched in Ag[13]. Molecular-dynamics simulations of nanoparticle growth by means of atomistic models agree with this observation[6,14,15]. In fact, simulating the deposition of Ag atoms onto Pd clusters leads to the formation of Pd@Ag core-shell structures[14]. On the other hand, Pd atoms deposited on Ag clusters mostly tend to incorporate inside the cluster[6].

Global optimization studies of Ag-Pd nanoparticles have been limited to small sizes, up to 60 atoms[16–18]. Their results confirm that cluster surfaces are greatly enriched in Ag, for all relevant cluster shapes. However, a systematic study of the equilibrium segregation profiles in Ag-Pd nanoparticles is still lacking, especially for what concerns diameters of at least 2-3 nm, that are of greater interest in experiments[13].

In this paper we consider magic sizes for fcc truncated octahedral (TO), icosahedral (Ih) and decahedral (Dh) nanoparticles and search for the most energetically stable chemical ordering arrangement for a series of compositions. Special attention is devoted to the surface and subsurface layers, which are the most relevant to determine the catalytic properties of these nanoparticles[10,11]. The stability of the low-energy chemical ordering patterns at increasing temperature is discussed, and the segregation profiles in the nanoparticles are compared also to those of bulk systems terminated by surfaces of different orientations.

2 Model and methods

The interactions between atoms in the Ag-Pd nanoparticles are modelled by the atomistic potential developed within the second-moment approximation to the tight-binding model[19–21]. Form and parameters of the potential can be

[a] *Physics Department, University of Genoa and CNR-IMEM, Via Dodecaneso 33, 16146, Genoa, Italy.*
[b] *Physics Department, University of Genoa and CNR-IMEM, Via Dodecaneso 33, 16146, Genoa, Italy, e-mail ferrando@fisica.unige.it*
[c] *National Research Council, Institute for Energetics and Interphases (CNR-IENI), Via De Marini 6, 16149 Genoa, Italy*

found in Ref. [17]. The parameters have been fitted on Density-Functional Theory calculations.

The optimal chemical order pattern has been searched for by global-optimization procedures. Specifically, we have used the basin-hopping algorithm (BH)[22,23]. The BH algorithm consists of a Metropolis Monte Carlo simulations in which local minimization is performed after each move. Since we are interested in determining the most favourable chemical ordering pattern within given geometric structures, we allow only exchange moves. This amounts to finding the best homotop[24] for any given size, structure and composition. In an exchange move, two atoms of different species are swapped. For all sizes and compositions, we made simulations using either random or tailored exchanges[7,25,26]. In a random exchange, the two atoms that are swapped are chosen randomly. In our tailored exchanges, the two atoms are chosen with different probabilities depending on their local environment. We have noticed that tailored exchanges biased towards intermixing lead to a somewhat more efficient location of low-energy chemical ordering patterns, even thought the improvement with respect to random exchanges is not as apparent as in phase-separating systems such as Ag-Ni or Ag-Cu. For each size and composition we have performed at least 5 independent runs on $5\ 10^5$ steps. The temperature used in the Metropolis procedure was quite low, with the most efficient optimization being those at 100 or 200 K. This is due to the rather small energy separation between homotops.

Monte Carlo simulations at higher temperatures have been used to check the stability of the optimal chemical ordering patterns within each given geometric structure with increasing temperature. These have been performed by the Metropolis algorithm allowing both exchange and local relaxation moves. We have also verified by Monte Carlo simulations with periodic boundary conditions that our model is able to reproduce the disordered phase of bulk crystals.

Thermodynamic calculations of surface composition for the corresponding bulk alloys are carried out by means of the multilayer thermodynamic model developed by Strohl and King[27].

In the following we consider three different geometric structures at selected magic sizes. Specifically, we consider an fcc TO of 586 atoms, an Ih of 561 atoms, and a Marks Dh[28,29] of 434 atoms. These structural motifs are in competition in the size range below 10^3 atoms. Our magic structures have been shown to be of remarkable energetic stability for both pure Ag and pure Pd[29]. They are shown in Fig. 1. For each geometric shape we consider compositions with 75 at.%, 50 at.% and 25 at.% Ag content. Moreover, we analyze in some detail the case in which a single Pd impurity is hosted in an Ag-rich matrix.

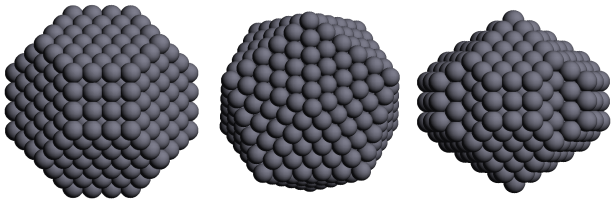

Fig. 1 From left to right: truncated octahedron of 586 atoms, icosahedron of 561 atoms and Marks decahedron of 434 atoms

3 Global optimization results

3.1 Ag-rich compositions

We consider first compositions that are close to 75 at.% Ag. Specifically, we consider the TO, Ih and Dh structures of compositions $Ag_{440}Pd_{146}$, $Ag_{421}Pd_{140}$ and $Ag_{325}Pd_{109}$, respectively. The lowest-energy chemical ordering patterns for the three structures are shown in Fig. 2.

Some features of chemical ordering are common to all motifs – the nanoparticle surface shell contains almost exclusively Ag, and the subsurface atomic shell is enriched in Pd with respect to the internal part of the nanoparticle (this behaviour, which is common to all compositions, is quantitatively analyzed in the final discussion below).

However the three structural motifs display also some specific behaviours. While in fcc and Ih nanoparticles the surface shell contains Ag atoms only, in the Dh nanoparticle, a few Pd atoms are visible at the cluster surface. They occupy the central sites at the bottom of Marks reentrances (see Fig. 2) and also a few sites on (111)-like facets.

Other specific behaviours are due to the existence of fivefold symmetry axes in Ih and Dh structures. In the pictures of the middle column of Fig. 2, it can be seen that there is Pd enrichment also along the fivefold symmetry axes.

Pd enrichment in subsurface and fivefold-axis sites can be qualitatively understood by considering the energetics of a single Pd impurity in an Ag host nanoparticle[6]. In Table 1 we report the data for the energetics and the local pressure acting on the impurity at different sites of the host TO, Ih and Dh Ag nanoparticles. We note that the atomic radius of Pd atoms is smaller than that of Ag atoms, so that we can expect that the substitution of Ag atoms with Pd atoms should allow the release of compressive strain, or the increase of tensile strain[7].

Surface sites are highly disfavoured, the more at decreasing coordination. Therefore the best surface sites are in the middle of (111) facets in TO and Ih structures, and at the bottom of the Marks reentrance in the Dh structure. Surface sites have always negative pressure that correspond to the tendency of surface atoms to contract in metals.

In the fcc TO structure, the most favourable internal sites are those that are placed just one atomic layer below the sur-

face (subsurface sites). In the pure Ag TO, pressures in subsurface sites are positive and larger than in inner sites, indicating a rather strong compression of subsurface atoms. When the Pd impurity is substituted at any given site, the pressure drops down to negative values, that are more negative in central sites than in subsurface sites. As a result, placing the Pd impurity in subsurface sites allow a better strain release than placing it in the inner part of the nanoparticle.

In pure Ag Dh structures, also the sites in the fivefold symmetry axis present rather large positive pressures, especially the two subvertex sites. As a result, both subsurface sites and sites in the symmetry axis benefit by a substitution with Pd impurities. The most favourable site is the subvertex site.

Ih structures present a more complex behaviour that cannot be completely explained even qualitatively by the analysis of the behaviour of a single Pd impurity. In Ih structures, the most favourable site for a single Pd atom is the central site, whose local pressure is very high in pure Ag Ih. This is followed by its 12 nearest-neighbour sites, and then by sites along the fivefold symmetry axis. Subsurface sites are in competition with off-axis inner sites. However, also in the Ih nanoparticle there is a subsurface enrichment when the palladium concentration exceeds the concentration needed to fill the central site and its neighbours.

Highly symmetric structures can be found for magic compositions. For example, a Dh structure whose chemical ordering preserves the full D_{5h} symmetry of the decahedron has been found for composition $Ag_{341}Pd_{93}$. This structure is shown in Fig. 3.

3.2 Intermediate compositions

In this case we consider TO, Ih and Dh structures of compositions $Ag_{293}Pd_{293}$, $Ag_{281}Pd_{280}$ and $Ag_{217}Pd_{217}$, respectively. The lowest-energy chemical ordering patterns for the three structures are shown in Fig. 4. The lowest energy structures present again a surface enrichment of Ag and a subsurface enrichment of Pd. However, several Pd atoms appear on the nanoparticle surfaces, and correspondingly, Ag atoms are found in the central part of the nanoparticle. Surface Pd atoms occupy inner sites of the (111) facets, and of the Marks reentrance in the decahedron. No Pd atoms are found on facet edges or vertices in TO and Ih structures, and very few in the Dh nanoparticle. Pd atoms in the (111) facets form regular patterns. A remarkable pattern is found in the Ih nanoparticle, in which Pd atoms occupy all corners of the inner triangles of the facets (see Fig. 4, middle row). Pd atoms prefer inner sites in (111) facets because of their higher coordination.

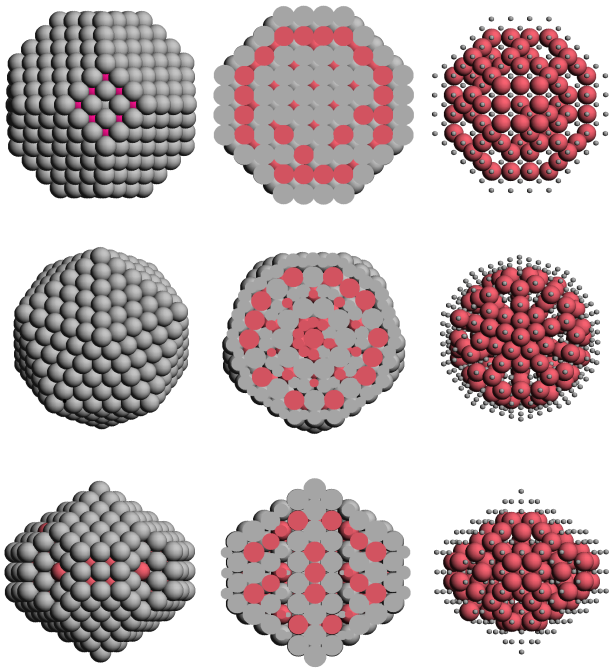

Fig. 2 Lowest-energy chemical ordering patterns for compositions with 75 at.% Ag. Each structure is shown in three views. Top row: fcc TO. Middle row: Ih. Bottom row: Dh. Ag and Pd atoms are shown in light grey and in pink, respectively. The pictures in the middle column show a cross-section of the nanoparticles in which the subsurface enrichment in Pd is evident. In the pictures of the right column Ag atoms are shown by small spheres.

3.3 Pd-rich compositions

Here we consider first compositions that are close to 25 at.% Ag (TO, Ih and Dh structures of compositions $Ag_{146}Pd_{440}$, $Ag_{140}Pd_{421}$ and $Ag_{109}Pd_{325}$, respectively). The lowest-energy chemical ordering patterns for the three structures are shown in Fig. 5.

In this case, the surface is still enriched in Ag, but with many Pd atoms that appear also in (100) facets and facet edges. The subsurface layer is almost exclusively of Pd atoms, while some Ag atoms are present in the central part of the nanoparticles. A remarkable pattern is found in the Ih nanoparticle. There, there is a central part made of 3 icosahedral shells (55 atoms) that contains only Pd atoms. In the fourth shell there are some Ag atoms, that occupy the centres of the facets of that shell, as shown in Fig. 6. Then there are no Ag atoms in the fifth shell (which is the subsurface shell) whereas a high concentration of Ag atoms is in the sixth shell (the surface shell).

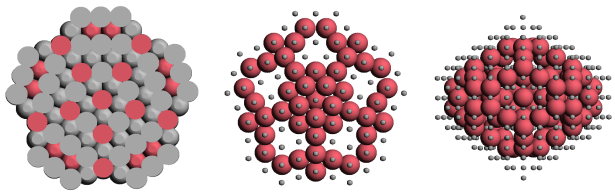

Fig. 3 Decahedral structure with highly symmetric chemical ordering found for composition $Ag_{341}Pd_{93}$. Symbols as in Fig. 2.

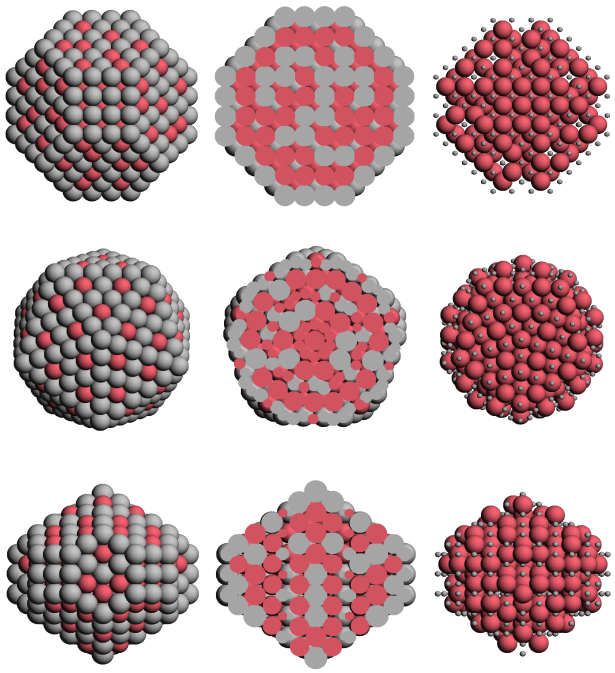

Fig. 4 Lowest-energy chemical ordering patterns for compositions with 50 at.% Ag. Each structure is shown in three views. Top row: fcc TO. Middle row: Ih. Bottom row: Dh. Symbols as in Fig. 2.

4 Discussion

Here we focus on the quantitative analysis of chemical ordering for the different structures and compositions. We first consider the lowest-energy structures that have been previously determined and then we consider finite-temperature effects by means of Monte Carlo simulations.

In order to analyze chemical ordering we have subdivided our structures in shells. For each structure, we consider the surface shell, the subsurface shell and the nanoparticle core. The subsurface shell is made of those atoms that, after removing the surface shell, appear on the nanoparticle surface. The nanoparticle core is defined as what remains after removing both surface and subsurface shells.

The compositions of the different shells in the lowest-energy structures are reported in Table 2. For each nanoparticle we count the total number of atoms in each shell (N_{surf}, N_{sub} and N_{core}) and the number of Pd atoms in each shell (N^{Pd}_{surf}, N^{Pd}_{sub} and N^{Pd}_{core}). The composition within each shell is analyzed in terms of the fractions of Pd atoms within the shell: $f^{Pd}_{surf} = N^{Pd}_{surf}/N_{surf}$, $f^{Pd}_{subs} = N^{Pd}_{subs}/N_{subs}$, and $f^{Pd}_{core} = N^{Pd}_{core}/N_{core}$, which are compared to the overall fraction of Pd atoms in the nanoparticle $f^{Pd}_{tot} = N^{Pd}/N$.

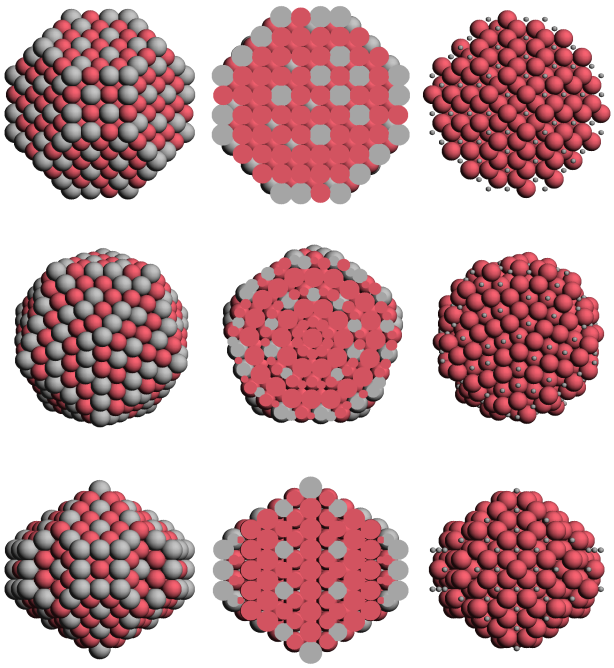

Fig. 5 Lowest-energy chemical ordering patterns for compositions with 25% Ag. Each structure is shown in three views. Top row: fcc TO. Middle row: Ih. Bottom row: Dh. Symbols as in Fig. 2.

The results in Table 2 show the expected Ag enrichment in the surface shell, which is essentially made of pure Ag when the overall Ag fraction is 0.75. However, the most remarkable result is the subsurface enrichment in Pd. One may expect that the composition of the subsurface shell is enriched in Pd with respect to the overall composition, simply because a notable number of Ag atoms is in the surface shell. However, the remarkable point is that the subsurface shell is significantly enriched in Pd *even compared to the core of the nanoparticle*. This effect is somewhat stronger in the TO structure, which does not contain fivefold axes. The Pd enrichment of the subsurface shell may have important consequences for those chemical reactions in which the role of subsurface sites has been demonstrated [10,11].

We have checked whether this subsurface Pd enrichment depends on the specific model that we are using. We have therefore repeated our calculations by means of a different parametrization of the potential, the one that was used in Refs. [6,14]. The results are qualitatively similar, with a signifi-

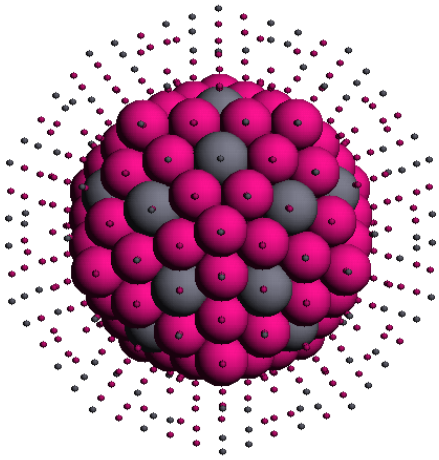

Fig. 6 Icosahedral nanoparticle of composition $Ag_{140}Pd_{421}$. Atoms of the subsurface and surface shells are shown as small spheres, so that the fourth shell can be seen. This is the only internal shell which contains Ag atoms.

cant subsurface enrichment in Pd. The main difference is that there is a somewhat higher number of Pd atoms in the surface shell.

Low-energy chemical ordering patterns determine the low-temperature properties of the nanoparticles. However, experiments are often performed at room temperature and above. Therefore it is important to check what is the effect of raising the temperature on the patterns that we have previously determined by global optimization. To this end, we have performed Monte Carlo simulations of 10^4 MC steps per particle in a temperature range up to 800 K, calculating the average subsurface and core compositions, in the case in which the overall Pd fraction is $f_{tot}^{Pd} = 0.25$. The results are reported in Fig. 7 and show that even though subsurface Pd enrichment decreases with temperature, it is still significant in the whole range considered in the simulations.

An interesting comparison can be made between segregation in nanoparticles and thermodynamic aspects of segregation at bulk surfaces. We adopt a multilayer thermodynamic model developed by Strohl and King[27] to analyze the segregation behaviour in the bulk alloys with $f_{tot}^{Pd} = 0.25$ and 0.50 for $T = 773$ K. The thermodynamic model uses as inputs the Ag-Pd phase diagram, the optimized thermodynamic data on the Gibbs free energy of the fcc solid phase[30], the surface energy data[31] and the molar volumes[32]of Ag and Pd pure components. For both alloys, the calculations of surface composition were carried out for two layers, i.e. the topmost and the subsurface atomic layers, taking into account the (100) and (111) orientations and the relation between the corresponding surface energies. The results are reported in Table 3. The calculations of surface composition for $f_{tot}^{Pd} = 0.25$ and 0.50 suggest a strong segregation of Ag atoms at the topmost layer and a subsurface enrichment in Pd, indicating so called *inverse* segregation. The degree of Ag surface segregation is slightly higher for the (100) surface, while subsurface inverse segregation is slightly higher for the (111) orientation. The results obtained are in qualitative agreement with similar results reported in[33]. Comparison with experiments on bulk samples is not straightforward because contradictory results are found in the literature for what concerns surface compositions, from Pd surface enrichment[34], to bulk composition[35], to weak Ag enrichment[36–38] and to strong Ag segregation[39,40].

Comparing results in bulk and nanoparticles, we can see that the subsurface enrichment is stronger at the nanoscale. In fact, the difference in composition between subsurface layer and inner part of the nanoparticle is larger than the difference in composition between the subsurface layer and the internal part of a bulk crystal. This nanoscale effect is due to the presence of a non-negligible proportion of edge and vertex sites. In fact, the most favourable sites for Pd impurities are those below edges and vertices (see Table 1).

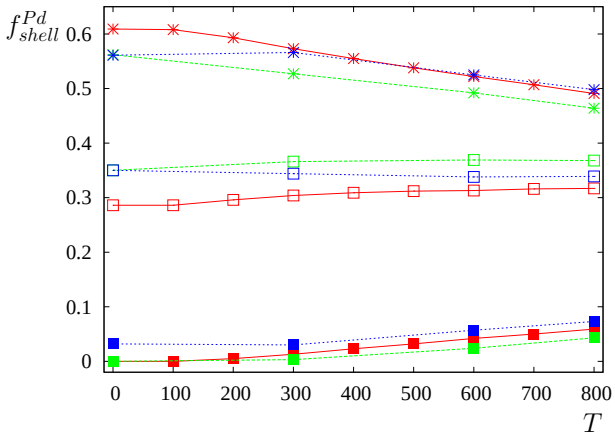

Fig. 7 Temperature dependence of the composition of the different shells as obtained by Monte Carlo simulations. Asterisks correspond to f_{subs}^{Pd}, open squares to f_{core}^{Pd} and full squares to f_{surf}^{Pd}. Red symbols refer to the fcc TO, green symbols to the Ih and blue symbols to the Dh. The overall fraction of Pd is $f_{tot}^{Pd} \simeq 0.25$.

5 Conclusions

The optimization of chemical ordering in magic-size Ag-Pd nanoalloys has singled out a behaviour whose main features are common to the different geometric structures (fcc, Ih and Dh nanoparticles) and to the different composition, from Ag-

rich to Pd-rich. These common features are the expected Ag enrichment of the surface, and, more important, a neat subsurface enrichment in Pd. Ag-Pd nanoparticles therefore present always a three-shell chemical ordering pattern in which the surface shell (of monoatomic thickness) is strongly enriched in Ag, the subsurface shell (of monoatomic thickness) is strongly enriched in Pd, while the inner part of the nanoparticle is rather weakly enriched in Pd. This behaviour is more pronounced in fcc nanoparticles, because in Ih and Dh nanoparticles also the inner sites in fivefold symmetry axes are enriched in Pd. Our simulations show also that the subsurface Pd enrichment slowly decreases with temperature, but it is still significant well above room temperature.

The chemical ordering pattern of Ag-Pd can be qualitatively rationalized in terms of the energetics of single Pd impurities in an Ag host nanoparticle. The inclusion of the Pd impurity at subsurface sites, or at sites of fivefold axes induces a better strain release with energetic advantages. On the other hand, surface sites are disfavoured because of their low coordination.

The most favourable chemical ordering patterns of AgPd nanoparticles of different shapes have been found by an atomistic model whose accuracy was previously tested against DFT calculations for smaller nanoparticle sizes [17]. We remark that in each of the nanoparticles considered here, there are many homotops that are very close in energy (few hundredth eV) to the lowest-energy minimum that we have found, and that our model is not likely to be accurate enough to correctly classify their energetic ordering. However, all these homotops share the same type of chemical ordering pattern, with Ag surface enrichment and Pd subsurface enrichment, so that they are essentially equivalent to each other from the experimental point of view. On the other hand, homotops that do not present Ag surface enrichment and/or Pd subsurface enrichment are much higher in energy, by several eV, and in this case our model is accurate enough to clearly distinguish between them.

Finally we remark that our findings can be relevant to the understanding of the catalytic activity of Ag-Pd nanoparticles, especially for those reactions for which a role of subsurface sites has been demonstrated.

The authors acknowledge support from the COST Action MP0903 “Nanoalloys as Advanced Materials: From Structure to Properties and Applications”.

References

1 R. Ferrando, J. Jellinek and R. L. Johnston, *Chem. Rev. (Washington, DC)*, 2008, **108**, 845–910.

2 C. Langlois, D. Alloyeau, Y. L. Bouar, A. Loiseau, T. Oikawa, C. Mottet and C. Ricolleau, *Faraday Disc.*, 2008, **138**, 375–391.

3 J.-I. Park, M. G. Kim, Y.-W. Jun, J. S. Lee, W.-R. Lee and J. Cheon, *J. Am. Chem. Soc*, 2004, **126**, 9072.

4 I. Parsina and F. Baletto, *J. Phys. Chem. C*, 2010, **114**, 1504–1511.

5 C. Langlois, Z. Y. Li, J. Yuan, D. Alloyeau, J. Nelayah, D. Bochicchio, R. Ferrando and C. Ricolleau, *Nanoscale*, 2012, **4**, 3381–3388.

6 F. Baletto, C. Mottet and R. Ferrando, *Phys. Rev. Lett.*, 2003, **90**, 135504.

7 D. Bochicchio and R. Ferrando, *Phys. Rev. B*, 2013, **87**, 165435.

8 F. Tournus, K. Sato, T. Epicier, T. J. Konno and V. Dupuis, *Phys. Rev. Lett.*, 2013, **110**, 055501.

9 A. J. Logsdail and R. L. Johnston, *J. Phys. Chem. C*, 2012, **116**, 23616.

10 N. A. Khan, S. Shaikhutdinov and H.-J. Freund, *Catal. Lett.*, 2006, **108**, 159.

11 S. Gonzalez, K. M. Neyman, S. Shaikhutdinov, H.-J. Freund and F. Illas, *J. Phys. Chem. C*, 2007, **111**, 6852.

12 L. G. Wang and A. Zunger, *Phys. Rev. B*, 2003, **67**, 092103.

13 A. Khan, A. Uhl, S. Shaikhutdinov and H.-J. Freund, *Surf. Sci.*, 2006, **600**, 1849.

14 F. Baletto, C. Mottet and R. Ferrando, *Phys. Rev. B*, 2002, **66**, 155420.

15 H. Y. Kim, H. G. Kim, D. H. Kim, and H. M. Lee, *J. Phys. Chem. C*, 2008, **112**, 17138.

16 G. Rossi, R. Ferrando, A. Rapallo, A. Fortunelli, B. C. Curley, L. D. Lloyd and R. L. Johnston, *J. Chem. Phys.*, 2005, **122**, 194309.

17 F. R. Negreiros, G. Barcaro, Z. Kuntová, G. Rossi, R. Ferrando and A. Fortunelli, *J. Chem. Phys.*, 2010, **132**, 234703.

18 X. Wua, Y. Wua, X. Kai, G. Wua and Y. Chen, *Chem. Phys.*, 2011, **390**, 36.

19 F. Cyrot-Lackmann and F. Ducastelle, *Phys. Rev. B*, 1971, **4**, 2406.

20 R. P. Gupta, *Phys. Rev. B*, 1981, **23**, 6265.

21 V. Rosato, M. Guillopé and B. Legrand, *Phil. Mag. A*, 1989, **59**, 321.

22 D. J. Wales and J. P. K. Doye, *J. Phys. Chem. A*, 1997, **101**, 5111.

23 G. Rossi and R. Ferrando, *J. Phys. Cond. Mat.*, 2009, **21**, 084208.

24 J. Jellinek and E. B. Krissinel, *Chem. Phys. Lett.*, 1996, **258**, 283.

25 F. Calvo, *Fadaray Discuss.*, 2008, **138**, 75.

26 K. Laasonen, E. Panizon, D. Bochicchio and R. Ferrando, *J. Phys. Chem. C*, 2013, **117**, 26405–26413.

27 J. Strohl and T. King, *J. Catal.*, 1989, **118**, 53.

28 L. D. Marks, *Rep. Prog. Phys.*, 1994, **57**, 603.
29 F. Baletto and R. Ferrando, *Rev. Mod. Phys.*, 2005, **77**, 371.
30 G. Ghosh, C. Kantner and G. Olson, *J. Phase Equil.*, 1999, **20**, 295.
31 W. Tyson and W. Miller, *Surf. Sci.*, 1977, **62**, 267.
32 X.-G. Lu, M. Selleby and B. Sundman, *Computer Coupling Phase Diagr. Thermochem.*, 2005, **29**, 68.
33 L. Mezey and J. Giber, *Surf. Sci.*, 1982, **117**, 220.
34 R. Moss and D. Thomas, *J. Catal.*, 1967, **8**, 162.
35 K. Christmann, *Thin Solid Films*, 1977, **46**, 249.
36 B. Wood and H. Wise, *Surf. Sci.*, 1975, 151.
37 G. Schwartz, *Surf. Sci.*, 1978, **76**, 113.
38 F. Reniers, M. Delplancke, A. Asskali, M. Jardinier-Offergeld and F. Bouillon, *Appl. Surf. Sci.*, 1994, **81**, 151.
39 R. Bouwmans, G. Lippits and W. Sachtler, *J. Catal.*, 1972, **25**, 350.
40 F. Kuijers and V. Ponec, *J. Catal.*, 1979, **60**, 100.

Table 1 Energetics and local pressure of a single Pd impurity at different sites in host Ag nanoparticles. P_{Ag} is the local pressure at the site when occupied by an Ag atom, whereas P_{imp} is the local pressure when the same site is occupied by the Pd impurity. Energies are given in eV and pressures are given in GPa. E_{imp} is the energy difference between the nanoparticle with the impurity at a given site, and the same nanoparticle with the impurity at the central site (for which $E_{imp} = 0$).

structure	shell	position	P_{Ag}	P_{imp}	E_{imp}
fcc TO	surface	vertex	-2.95	-2.66	0.586
		edge	-2.88	-2.92	0.492
		(100) facet	-3.14	-3.30	0.349
		(111) facet	-2.09	-3.89	0.298
	subsurface	subvertex	4.64	-0.75	-0.042
		subedge	2.86	-2.63	-0.040
		sub (111)	1.93	-3.68	-0.022
		sub (100)	2.60	-2.84	-0.021
	core	center	0.53	-5.26	0.000
		2nd layer	0.85	-4.91	-0.016
Ih	surface	vertex	-2.99	-2.63	0.895
		edge	-4.88	-5.85	0.713
		facet	-5.37	-7.08	0.630
	subsurface	subvertex	7.39	2.26	0.201
		subedge	2.06	-3.33	0.265
		subfacet	0.88	-4.63	0.279
	core	center	35.48	32.25	0.000
		axis 1	14.33	8.71	0.120
		axis 2	8.67	3.20	0.179
		off-axis 1	6.09	0.09	0.210
		off-axis 2	2.89	-2.87	0.250
Dh	surface	vertex	-2.45	-1.95	0.648
		(100) facet	-2.55	-2.54	0.368
		(111) facet	-2.41	-4.12	0.337
		reentrance	3.16	-4.23	0.234
	subsurface	subvertex	7.02	1.85	-0.043
		subedge	3.20	-2.26	-0.003
		sub (111)	1.75	-3.92	0.012
		sub (100)	4.69	-0.71	-0.008
	core	center	3.10	-2.47	0.000
		off-axis	1.36	-4.36	0.023

Table 2 Pd atomic fraction in the surface shell (f^{Pd}_{surf}), in the subsurface shell (f^{Pd}_{surf}) and in the core (f^{Pd}_{core}) for the lowest-energy chemical ordering patterns of the different structures, compared to the overall Pd atomic fraction (f^{Pd}_{tot}) in the nanoparticle.

structure	f^{Pd}_{tot}	f^{Pd}_{surf}	f^{Pd}_{subs}	f^{Pd}_{core}
fcc TO	0.249	0.000	0.609	0.286
Ih	0.250	0.000	0.562	0.333
Dh	0.251	0.032	0.561	0.350
fcc TO	0.500	0.254	0.816	0.586
Ih	0.499	0.238	0.747	0.674
Dh	0.500	0.306	0.780	0.575
fcc TO	0.751	0.552	1.000	0.829
Ih	0.750	0.520	1.000	0.871
Dh	0.749	0.563	1.000	0.850

Table 3 Pd atomic fraction of surface and subsurface atomic layers in bulk Ag-Pd fcc crystals with (111) and (100) surfaces. The fraction of Pd atoms in the inner part of the crystals f^{Pd}_{core} coincides with the overall fraction f^{Pd}_{tot}. The data are calculated at the temperature of 773 K.

f^{Pd}_{tot}	orientation	f^{Pd}_{surf}	f^{Pd}_{subs}
0.250	(100)	$2\ 10^{-3}$	0.347
	(111)	$3\ 10^{-3}$	0.357
0.500	(100)	$6\ 10^{-3}$	0.561
	(111)	$9\ 10^{-3}$	0.582